Clinical Biomechanics 134 (2026) 106792



Contents lists available at ScienceDirect

Clinical Biomechanics

journal homepage: www.elsevier.com/locate/clinbiomech



Three-dimensional analysis of interbody cage-apophyseal ring contact to predict endplate subsidence following transforaminal interbody fusion

Kay A. Raftery [a], Hannah Levy [b], Lea Adamson [c], Christopher Magera [b], Brett Freedman [b], Nicolas Newell [a,*]

[a] Department of Bioengineering, Imperial College London, UK
[b] Department of Orthopaedic Surgery, Mayo Clinic, Rochester, USA
[c] Faculty of Medicine, Imperial College London, UK

ARTICLE INFO

Keywords:
Lumbar interbody fusion
Vertebra
Endplate
Subsidence
Apophyseal ring
Interbody cage

ABSTRACT

Background: There is a higher risk of subsidence following transforaminal lumbar interbody fusion (TLIF) relative to other approaches. Decreased subsidence risk is associated with anterior cage placement, speculated to be because of increased apophyseal ring contact. However, this hypothesis is largely based on in vitro evidence and, to date, has not been investigated in a clinical cohort.

Methods: Pre-operative and post-operative computed tomography (CT) images from 42 TLIF patients were used to segment the endplate and cages. The apophyseal ring boundary was manually landmarked for each endplate. The pre-operative endplates were rigidly registered with the post-operative cage position, and an iterative closest point approach was used to calculate the contact area between the cage, apophyseal ring, and endplate. Subsidence was categorised based on severity (No Subsidence: <2 mm; Moderate Subsidence: 2-4 mm; Severe Subsidence: ≥4 mm) from post-operative CT.

Findings: Apophyseal ring contact was significantly lower in both Moderate and Severe Subsidence, relative to No Subsidence (Moderate: $-19.6 \pm 7.0\%$; Severe: $-21.5 \pm 6.5\%$; $P < 0.05$), and negatively correlated with subsidence depth ($P < 0.05$). Injury risk analysis demonstrated that a 50% subsidence risk was associated with 45.7% (38.4–53.6%) apophyseal ring contact. Suprajacent endplate apophyseal ring contact, but not subjacent, was significantly predictive of subsidence at the respective endplate ($P < 0.05$).

Interpretation: The risk of subsidence in TLIF patients can be mitigated by ensuring that at least half of the interbody cage surface area is in contact with the peripheral endplate rim, particularly at the endplate superior to the cage.

1. Introduction

Surgical management of lower back pain is becoming an increasing healthcare burden in the United Kingdom (UK), costing the National Health Service an estimated £1.6 billion a year (Maniadakis and Gray, 2000; Rushton et al., 2015). Spinal fusion is the most prevalent procedure (Provaggi et al., 2018; Sivasubramaniam et al., 2015), whereby an interbody device is implanted into the intervertebral disc space to encourage bony fusion between two vertebrae. This offers indirect decompression of nerve roots and maximisation of segmental lordosis to manage various symptomatic spinal degenerative conditions.

Multiple interbody fusion approaches have emerged, albeit no conclusive evidence favours a particular approach regarding intra-operative efficiency, post-operative complications, and fusion outcome (Mobbs et al., 2015). However, the small surgical window and interbody cage footprint used in transforaminal lumbar interbody fusion (TLIF) may result in inaccurate cage placement and insufficient congruency with the endplate (Lee et al., 2017). These disadvantages manifest in a 37.4% subsidence risk, estimated to be on average 22% higher than anterior (ALIF), posterior, (PLIF) and oblique (OLIF) approaches (Lee et al., 2017; Lin et al., 2018). Subsidence describes the event of excessive interbody cage settling into the underlying bone, and is associated with reduced fusion rates (Satake et al., 2017) or non-union (Levy et al., 2024), loss of intervertebral height at the index level (Chen et al., 2005), and recurrence of symptoms (Fukuta et al., 2011).

Decreased subsidence risk in TLIF is associated with anterior cage

* Corresponding author at: Department of Bioengineering, Imperial College London, White City Campus, London W12 0BZ, United Kingdom.
E-mail address: n.newell09@imperial.ac.uk (N. Newell).

https://doi.org/10.1016/j.clinbiomech.2026.106792
Received 17 October 2025; Accepted 12 February 2026
Available online 13 February 2026
0268-0033/© 2026 The Authors. Published by Elsevier Ltd. This is an open access article under the CC BY license (http://creativecommons.org/licenses/by/4.0/).

placement (Amorim-Barbosa et al., 2022; Levy et al., 2024; Yao et al., 2020). This is speculated to be because anterior placement is synonymous with greater contact with the apophyseal ring (Rickert et al., 2023). The apophyseal ring is a peripheral ring of cortical bone at the endplate, distinguishable from the central cortex, which is largely supported by cancellous bone (Grant et al., 2001; Grant et al., 2002).

Previous ex vivo biomechanical studies have reported a greater failure load, work to subsidence, and apparent stiffness when compressing endplates using cages which span the apophyseal ring relative to those placed centrally (Andriamifidy et al., 2024; Briski et al., 2017; Palepu et al., 2019a). However, it is more evident that post-operative subsidence is a temporal consequence of continuous remodelling at the cage-endplate boundary, creep, and microfracture accumulation in the cancellous bone (Fyhrie and Schaffler, 1994). Despite this, no clinical study to date has quantified the contact area between the interbody cage and the apophyseal ring to predict post-operative subsidence. This would allow the potentially influential roles of complex dynamic loading and bone remodelling to be accounted for, and ultimately is necessary to evaluate whether targeting localised stronger regions of the endplate is a worthwhile consideration in practical efforts to reduce subsidence risk.

Therefore, the aims of this retrospective clinical-cohort study were to:

1) Compare apophyseal ring-interbody cage contact areas at the suprajacent endplate, subjacent endplate, and whole index level in TLIF patients categorised by the amount of subsidence measured post-operatively.
2) Evaluate suprajacent, subjacent, and whole index level apophyseal ring-interbody cage contact area as a predictive measure of subsidence incidence and depth.

2. Methods

2.1. Patient cohort

Patient information and radiographic images were retrospectively obtained from a multi-centre academic institution. Ethical approval was obtained from the Institutional Review Board (Mayo Clinic, Rochester, USA; approval no: 23–003878) and the Imperial College Science, Engineering and Technology Research Ethics Committee (London, UK; approval no. 7542982). Informed consent was not required for the purposes of this study. The STROBE cohort checklist was used when writing this report (von Elm et al., 2014).

167 patients older than 18 years of age undergoing TLIF surgery for lumbar spondylosis, neural claudication, or symptomatic disc degeneration between 2014 and 2021 with no record of traumatic injury, malignancy, or infection were screened for inclusion (Supplementary Fig. 1).

Patients with a radiographic follow-up less than six months after surgery or incomplete imaging records were excluded. A six-month follow-up threshold was standard according to routine clinical practice at the institution, and was considered sufficient to capture subsidence cases, since 70% of subsidence events are thought to occur by 8 months post-operation (Choi and Sung, 2006). Other contraindications were fusion at the L5-S1 index, multiple interbody or instrumented levels, and any prior fusion surgery or instrumented decompression, as these surgical factors are known to increase the risk of subsidence due to alterations in the mechanical environment (Hu et al., 2019; Yoo et al., 2022; Zhang et al., 2025). Due to the radiolucency of polyetheretherketone (PEEK) interbody cages, only fusions using titanium interbody cages were included.

2.2. Operative treatment

The lumbar spine was approached via the posterior mid-line and the operative index level was confirmed using fluoroscopy. Exposure of the transverse processes was achieved to enable decortication. A unilateral facetectomy was performed, additionally removing the ventral facet capsule and ligamentum flavum. A box annulotomy through the posterolateral annulus and preparation of the disc space was then performed. Paddle shavers and curettes were used to thoroughly prepare the endplates, whilst taking care to avoid breaching the cortical bone, of which was recorded after visual inspection of intra-operative or immediate post-operative standing radiographs. After sufficient preparation, the interbody cage was inserted into the intervertebral space, as anteriorly as possible, and with fluoroscopic guidance. The cages used were either banana- or bullet-shaped. Fusion was attempted in the disc space, posterolateral gutter, and contralateral facet. The interbody cage was packed with autograft or cancellous allograft prior to insertion. If bone morphogenic protein (BMP) was used, the anterior disc space was filled before interbody cage insertion, with additional placement in the lateral gutters. All patients underwent posterolateral fixation with pedicle screws.

2.3. Patient, surgical, and radiographical variables

All patient demographics, pre-operative indications, surgical factors, post-operative outcomes, and radiographic measurements were retrospectively obtained, further details of which can be found in (Levy, 2025; Levy et al., 2024). Briefly, centre point ratio (CPR) was measured using standing lateral radiographs, defined as the ratio of the distance between the cage centroid and the posterior extent of the subjacent endplate, divided by the anterior-posterior length of the subjacent endplate.

Pre-operative computed tomography (CT) images were used to calculate L3 Hounsfield units (HU), defined as the average of the superior, middle, and inferior axial slices of the L3 vertebral body. L3 was used to ensure that the HU was largely indicative of the bone quality proximal to the index level, whilst avoiding degenerative changes common in lower lumbar levels.

Disc height was measured as the average of the anterior, central, and posterior disc height at the mid-sagittal view of the pre-operative CT. The height of the interbody cage was divided by the disc height to calculate the interbody cage height-disc height ratio. All other patient variables were measured via routine chart review.

Subsidence measurements were conducted by up to six independent reviewers (Levy, 2025; Levy et al., 2024). Briefly, the mid-coronal and mid-sagittal slices of the post-operative CT images were used to measure the maximum depth of the cage with respect to the supra- and subjacent endplate. Measurements in the sagittal and coronal plane, and between raters, were averaged to generate the final measurements.

The magnitude of subsidence at each endplate was categorised (No Subsidence: <2 mm; Moderate Subsidence: ≥ 2 and <4 mm; Severe Subsidence: ≥ 4 mm) (Pinter et al., 2023a; Pinter et al., 2023b). The cohort was additionally categorised based on the maximum amount of subsidence that the patient sustained across the index level.

2.4. Segmentation pipeline

The interbody cage and the supra- and subjacent endplate regions from both pre-operative and post-operative CT images (140 kVp, 280 mAs, in-plane resolution: 0.293 mm^2, slice thickness: 0.75 mm) were segmented at the level of fusion. Segmentation was performed by two raters familiar with spinal anatomy and radiography (KR and LA). To segment the pre-operative endplates, a semi-automated approach was employed using a commercial software (Mimics v25.0, Materialise HQ, Leuven, Belgium) which relied on initial auto-thresholding of HU to isolate bone from soft tissue, the volume of which was manually refined and extended in the local axial direction (depth: 5-10 mm) to ensure that any areas of high concavity were captured (Fig. 1A). For post-operative endplates, additional manual segmentation was implemented where

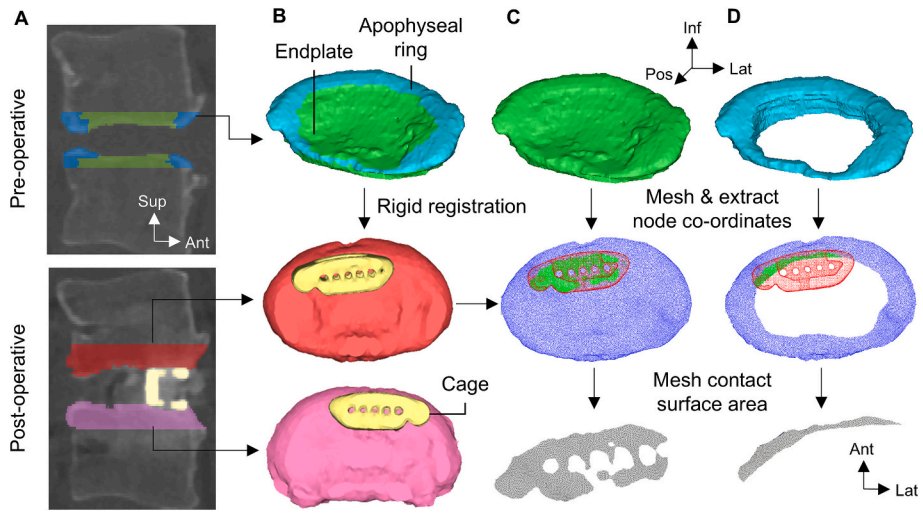


Fig. 1. Workflow of (A) endplate segmentation and (B) cage registration onto the suprajacent (red) and subjacent (pink) endplates to generate the (C) cage-endplate and (D) cage-apophyseal ring contact area. Ant: anterior; pos = posterior; lat = lateral; sup = superior; inf = inferior. (For interpretation of the references to colour in this figure legend, the reader is referred to the web version of this article.)

metal-related artefacts and areas of bony fusion prevented reliable auto-thresholding.

To align the pre-operative endplate with the interbody cage, the pre-operative endplate was transformed into the post-operative co-ordinate system. To do this, each supra- and subjacent pre-operative endplate object was aligned to the respective endplate in the post-operative CT scan, using an automatic rigid registration tool in Mimics (minimum point distance filter: 1 mm) (Fig. 1B). This generated patient- and endplate-specific transformation matrices. Three-dimensional surface meshes of the transformed pre-operative endplate objects were then generated in 3-Matic (Materialise HQ, Leuven, Belgium). A maximum edge length of 0.3 mm was chosen for the mesh size, as this was comparable to the CT in-plane resolution (0.293 mm).

2.5. Quantification of cage-endplate and cage-apophyseal ring contact area

The nodal co-ordinates for both the cage and transformed preoperative endplate meshes were used as an input for a custom-written MATLAB script (v2023a, MathWorks, Natick, MA, US) to calculate the cage-endplate contact area (Fig. 1C), which represented the load-bearing area at the endplate produced by cage contact, accounting for any mismatch between surfaces. An iterative closest point approach was employed with a Euclidian distance threshold of 0.3 mm to determine whether any two three-dimensional co-ordinate pairs ("endplate" co-ordinates and "cage" co-ordinates) were in contact. The resulting point cloud of endplate co-ordinates which were defined as in contact with the cage was meshed using a ball-pivoting surface reconstruction approach (PyMeshLab v2023.12 (Muntoni and Cignoni, 2025)). The surface area of the resulting mesh for both the supra- and subjacent endplates was then calculated.

To quantify the cage contact with the apophyseal ring only, the boundary of the apophyseal ring was manually segmented in Mimics, using the rendered object of the pre-operative endplate as a geometrical guide. The boundary was visually identifiable across the endplate circumference as an inflection point in the three-dimensional curvature from the convex peripheral bone to the concave medial endplate (Fig. 1B,D). Similar approaches to define the apophyseal ring have been previously documented (Palepu et al., 2019b; Sun et al., 2018; Wang et al., 2023). To enhance repeatability of the segmentation, each boundary was replicated by one rater three times, at least 24 h apart, and blinded to all previous tests. The average boundary was used in subsequent analyses (Supplementary Fig. 2).

To create the apophyseal ring surface co-ordinates, the boundary co-ordinates were interpolated in MATLAB and any endplate surface co-ordinates which were located medial to this boundary were removed (Fig. 1D). The pipeline to quantify surface contact was repeated to calculate the cage-apophyseal ring contact area, creating a mesh representing the load-bearing area of the apophyseal ring only. Apophyseal ring contact percentage was calculated by normalising the cage-apophyseal ring contact area to the total cage-endplate contact area.

Cage-endplate contact area, cage-apophyseal ring contact area, and apophyseal ring contact percentage were recorded separately for the supra- and subjacent endplate. To additionally evaluate contact at the whole index level, the sum of both endplate contact areas and average relative apophyseal ring contact percentage were calculated.

2.6. Measurement reliability

The repeatability of the segmentation, mesh generation, and contact area quantification pipeline between the segmentations of both raters was assessed. Both raters performed segmentation on three randomly chosen patients to separately generate cage-endplate and cage-apophyseal ring contact area meshes. Intra-rater reliability was further assessed in one rater (KR), where the segmentation and analysis for the same three patients were repeated six weeks later. Reliability was assessed using intra-class correlation coefficient (ICC), where >0.75 and >0.9 were considered good and excellent reliability, respectively (Koo and Li, 2016).

2.7. Quantification of HU under the cage-endplate contact site

The HU corresponding to each voxel was extracted from each pre-operative endplate mask (Fig. 2A). For each endplate, the patient-specific transformation matrix was applied to transform the HU field into the post-operative space.

A custom-written MATLAB code identified the HU surface voxels which were superimposing the cage-endplate contact area, using a nearest-neighbour approach. The surface area was extended perpendicular to the endplate plane by calculating the normal vector (Fig. 2B). For each HU surface voxel, the vector was used to translate 0.2 mm until a 2 mm magnitude was reached (Fig. 2C). HU voxels were identified using an iterative closest point approach (threshold distance: 0.3 mm). A 2 mm depth was chosen, since previous work has shown that a 1.25–2.5 mm endplate volume is the strongest predictor of subsidence, relative to other volumetric HU measures (Di et al., 2023).

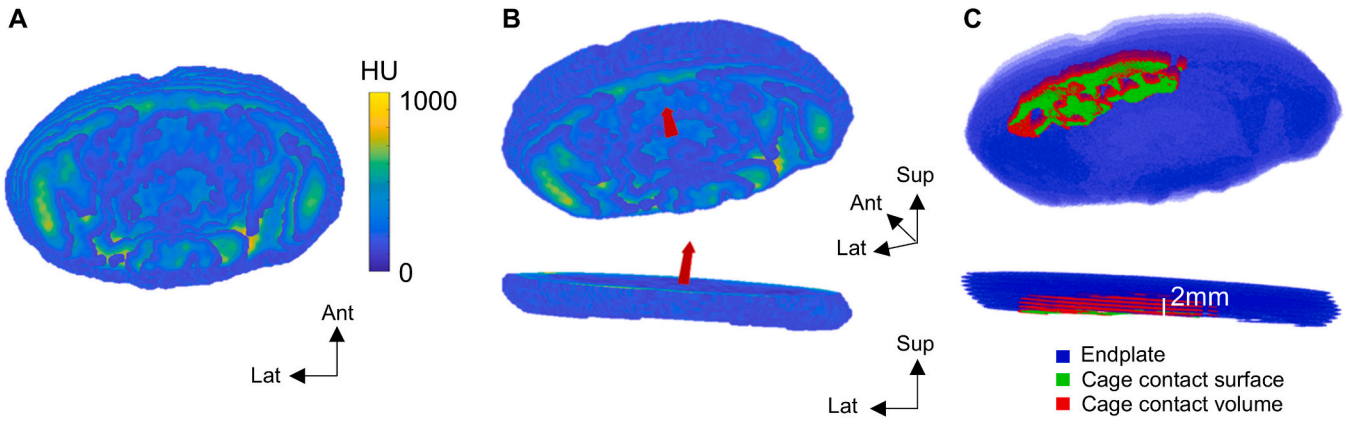


Fig. 2. (A) Endplate Hounsfield unit (HU) map. (B) Identification of the vector perpendicular to the endplate plane (red arrow) to calculate a (C) 2 mm HU volume underlying the cage contact surface. Ant: anterior; lat = lateral; sup = superior; inf = inferior. (For interpretation of the references to colour in this figure legend, the reader is referred to the web version of this article.)

2.8. Statistical analysis

Groupwise comparison tests were performed in Prism (v10.0.2, GraphPad Software, San Diego, California, United States). Groups were initially assessed for normality using Shapiro-Wilk tests, and Brown-Forsythe tests were conducted to assess homoscedasticity. To assess differences between subsidence groups, one-way ANOVA with Tukey's post-hoc was performed. Where normality and equal variance were violated, a Kruskal-Wallis test with Dunn's post-hoc was performed; where equal variance alone was violated, Welch's ANOVA was performed.

Regression analyses were performed in SPSS (v25, IBM, Chicago, IL). Contact variables were added to a stepwise logistic regression model to predict maximum, suprajacent, and subjacent subsidence alongside patient and surgical factors which have previously been shown to be significant predictors of TLIF subsidence (Moderate Subsidence: cage length, cage width, cage type (bullet or banana), CPR; Severe Subsidence: cage length, cage width, cage height, CPR, L3 HU, index-level disc height, cage height to disc height ratio, BMP use (Levy et al., 2024)). A stepwise linear regression model to predict subsidence depth was additionally performed with all respective covariates. Multicollinearity between predictor variables were assessed with variance inflation factors, and normality and homoscedasticity were visually assessed by plotting the residuals.

2.8.1. Injury risk analysis

To quantify the risk of subsidence associated with apophyseal ring contact, an injury risk curve was developed in R (R Core Team, 2014) using parametric survival analysis (Supplementary Methods). The injury risk function is based on the log-logistic cumulative distribution function (Eq. (1)):

$$F(x) = \frac{1}{1 + \left[\frac{x}{\eta}\right]^{-\beta}} \quad (1)$$

Where x refers to the primary variable, η the scale parameter, and β the shape parameter. Due to the monotonic constraint of this function, the inverse of the sum apophyseal ring contact percentage was used as the primary variable, namely core region contact percentage (100 – apophyseal ring contact percentage). Subsidence outcomes were censored (Petitjean et al., 2015), whereby No Subsidence outcomes were right censored, since no event occurred at the measured apophyseal ring contact percentage, but it was unknown if greater core region contact would have resulted in injury. Moderate Subsidence or Severe Subsidence outcomes were left-censored, since the threshold of apophyseal ring contact required to cause injury was unknown.

The normalised confidence intervals (NCIS) of the injury curve were computed at discrete probability intervals (5%, 10%, 25%, 50%, 75%, 90%, 95%), where NCIS <0.5: "good", 0.5–1: "fair", 1–1.5: "marginal", >1.5: "unacceptable" (Yoganandan et al., 2020).

3. Results

3.1. Cohort definition

42 patients were indicated for this study (Table 1). The cage-apophyseal ring contact area and apophyseal ring contact percentage of the subjacent endplate (and subsequently the index level) within one patient were excluded in the Severe Subsidence group, due to an unreliable distinguishment of the boundary. The number of intra-operative endplate violation events was not significantly different between the subsidence groups (Fisher's exact $P > 0.29$).

Table 1
Patient groupings, age, gender (% male), and BMI for No Subsidence, Moderate Subsidence, and Severe Subsidence for the suprajacent endplate, subjacent endplate, and index level. a = significant difference with No Subsidence group, b = significant difference with Moderate Subsidence group. $^{**}P < 0.01$, $^{*}P < 0.05$.

N	No Subsidence (<2 mm)	Moderate Subsidence (2-4 mm)	Severe Subsidence (≥4 mm)
Suprajacent	8	22	12
Subjacent	14	12	16
Index	7	13	22
Age (SD)			
Suprajacent	57.4 (11.1)	68.1 (7.9)*[a]	68.1 (8.5)*[a]
Subjacent	60.6 (10.1)	71.1 (8.5)*[a]	67.0 (7.5)
Index	56.3 (11.4)	67.9 (8.5)*[a]	68.1 (7.7)**[a]
Gender (% male)			
Suprajacent	37.5	45.5	58.3
Subjacent	50.0	41.7	50.0
Index	42.9	38.5	54.5
BMI[1] (SD)			
Suprajacent	30.1 (4.1)	30.1 (4.9)	30.7 (7.4)
Subjacent	29.5 (3.4)	28.3 (5.1)	32.4 (6.6)
Index	31.3 (2.3)	27.2 (3.35)*[a]	31.8 (6.5)*[b]

[1] Body mass index.

3.2. Segmentation reliability

Between the two raters, the ICC for contact area (cage-endplate and cage-apophyseal ring) was 0.969 (95CI 0.903–0.991) ($P < 0.001$), and 0.887 (0.367–0.983) ($P < 0.01$) for apophyseal ring contact percentage. The root mean squared error (RMSE) was 26.3 mm^2 and 6.3%, respectively.

For the test-retest evaluation, the ICC was 0.996 (0.985–0.999) ($P < 0.001$) for contact area and 0.897 (0.508–0.984) ($P < 0.01$) for apophyseal ring contact percentage. The RMSE was 8.3 mm^2 and 5.3%, respectively. No bias was detected between ratings for both the inter-rater and test-retest evaluation (Supplementary Fig. 3).

3.3. Comparison between subsidence categories

When patients were categorised based on maximum subsidence across the index level, average cage-endplate contact area was significantly lower in Severe Subsidence relative to No Subsidence ($P < 0.05$) (Fig. 3A). Additionally, cage-apophyseal ring contact area and apophyseal ring contact percentage were significantly lower in both Moderate and Severe Subsidence relative to No Subsidence (Moderate: $-19.6 \pm 7.0\%$, $P < 0.05$; Severe: $-21.5 \pm 6.5\%$, $P < 0.01$) (Fig. 3B,C).

When patients were categorised based on maximum subsidence at the suprajacent or subjacent endplate only, significantly higher suprajacent cage-endplate and cage-apophyseal ring contact area was observed in the No Subsidence group, relative to Moderate and Severe Subsidence ($P < 0.05$) (Fig. 3D,E,J). However, apophyseal ring contact percentage was not significantly different ($P = 0.9$) (Fig. 3F). No significant differences were observed for any contact variable at the subjacent endplate only (Fig. 3G-I).

3.4. Prediction of subsidence incidence and depth

In the logistic regression model predicting any subsidence event (≥2 mm) occurring at the index level, reduced sum cage-endplate contact area, sum cage-apophyseal ring contact area, and sum apophyseal ring contact percentage were all significant univariate predictors ($P < 0.05$). The same effect was observed for suprajacent subsidence ($P < 0.05$), but not subjacent subsidence. In the stepwise model, the only significant multivariate predictor for subsidence at the suprajacent, subjacent, and whole index was cage length ($P < 0.01$), although sum apophyseal ring contact percentage remained in the final model (Table 2).

In the event of severe subsidence (≥4 mm), no contact variable at either endplate or the whole index level was a significant univariate predictor ($P > 0.057$). Significant multivariate predictors for apophyseal ring contact percentage were cage length, cage height, and L3 HU ($P < 0.05$) (Table 2).

At the index level, reduced sum cage-endplate contact area, sum cage-apophyseal ring contact area, and sum apophyseal ring contact percentage were all significant univariate predictors of subsidence depth ($P < 0.05$). However, only CPR, cage length, and L3 HU were significant multivariate predictors ($P < 0.05$) (Table 3).

At the supra- and subjacent endplates, subsidence depth was predicted by reduced sum cage-endplate contact area, sum cage-apophyseal ring contact area, and sum apophyseal ring contact percentage at the respective endplate ($P < 0.05$). However, in the stepwise model, suprajacent subsidence was best predicted by cage length and L3 HU ($P < 0.05$). Subjacent subsidence was best predicted by cage length and CPR ($P < 0.05$) (Table 3).

In the injury risk model, a 50% risk of subsidence was associated with a core endplate contact percentage of 54.3% (NCIS 46.4–61.6%) (Fig. 4), or an apophyseal ring contact percentage of 45.7% (NCIS 38.4–53.6%).

3.5. HU beneath the contact site

The HU beneath the interbody cage averaged across the index level was significantly higher in No Subsidence relative to Severe Subsidence ($+131.2 \pm 38.8$, $P < 0.01$). When considering the suprajacent endplate only, HU was significantly higher in No Subsidence relative to Severe

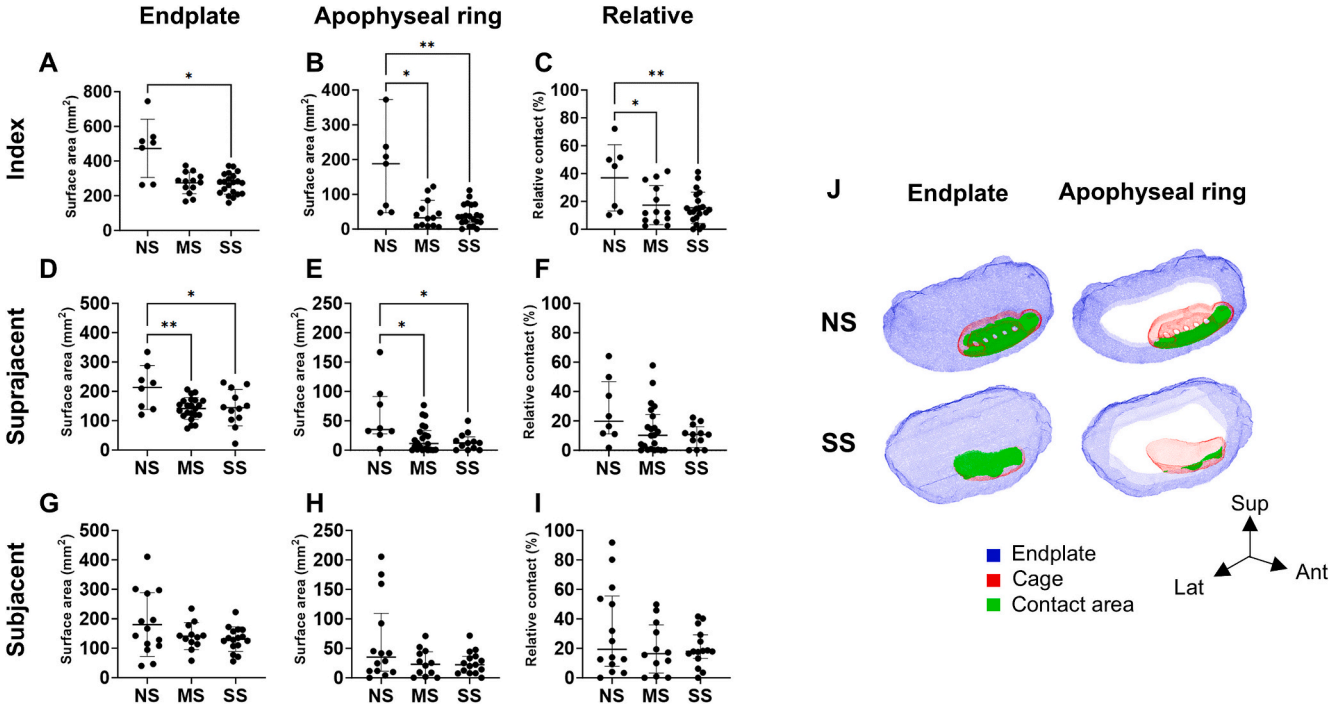


Fig. 3. (A,D,G) Cage-endplate contact area, (B,E,H) cage-apophyseal ring contact area, and (C,F,I) apophyseal ring contact percentage for the (A-C) whole index level, (D-F) the suprajacent endplate, and (G-I) the subjacent endplate. NS: No Subsidence, MS: Moderate Subsidence, SS: Severe Subsidence. Mean (SD) is shown for normally distributed data and median (inter-quartile range) is shown otherwise. (J) Depiction of apophyseal ring contact in a typical No Subsidence and Severe Subsidence endplate. Ant: anterior; lat = lateral; sup = superior. $^{**}P < 0.01$, $^{*}P < 0.05$.

Table 2
Univariate and multivariate logistic odds ratios (95CI) to predict subsidence severity. Note that variables which were not included in the final iteration of multivariate analysis, and covariates which were not considered for univariate analysis, are indicated by a dash. $^{**}P < 0.01$, $^{*}P < 0.05$ (bold typeface).

	> 2 mm (Moderate + Severe Subsidence)						> 4 mm (Severe Subsidence only)					
	Univariate			Multivariate			Univariate			Multivariate		
	Suprajacent	Subjacent	Index	Suprajacent	Subjacent	Index	Suprajacent	Subjacent	Index	Suprajacent	Subjacent	Index
Cage-endplate contact area	**0.976 (0.959–0.995)***	0.991 (0.981–1.001)	**0.980 (0.967–0.994)**	–	–	–	0.995 (0.983–1.007)	0.993 (0.982–1.003)	0.992 (0.985–1.000)	–	–	–
Cage-apophyseal ring contact area	**0.961 (0.931–0.993)***	0.981 (0.962–1.000)	**0.973 (0.953–0.993)**	–	–	–	0.975 (0.941–1.010)	0.987 (0.967–1.008)	0.987 (0.973–1.001)	–	–	–
Apophyseal ring contact %	**0.953 (0.911–0.998)***	0.974 (0.944–1.005)	**0.929 (0.877–0.93)***	–	–	0.927 (0.832–1.033)	0.963 (0.91–1.018)	0.985 (0.953–1.018)	0.964 (1.007)	–	–	–
Cage length	–	–	–	**0.441 (0.224–0.868)***	1.415 (0.812–2.465)	**0.438 (0.208–0.926)***	–	–	–	–	0.555 (0.302–1.018)	**0.724 (0.525–0.998)***
Cage height	–	–	–	–	–	–	–	–	–	–	**2.998 (1.062–8.462)***	2.175 (0.971–4.871)
Centre point ratio	–	–	–	–	–	–	–	–	–	–	< 0.0001 (< 0.0001–2.497)	–
L3 HU[1]	–	–	–	–	–	–	–	–	–	**0.972 (0.948–0.996)***	–	**0.963 (0.934–0.994)***
Cage height: disc height ratio	–	–	–	–	–	–	–	–	–	1.268 (0.875–1.837)	2.032 (0.977–4.226)	1.344 (0.877–2.058)

[1] Hounsfield unit.

Subsidence (+133.3 ± 39.0, $P < 0.01$). This was also the case for the subjacent endplate (+109.4 ± 43.3, $P < 0.05$).

Across the index level, apophyseal ring contact percentage was positively correlated with HU beneath the contact site, whilst controlling for global bone quality (L3 HU) (partial correlation coefficient: 0.460, $P < 0.01$). This effect was similarly observed for the subjacent endplate (0.587, $P < 0.001$), but not the suprajacent (0.189, $P = 0.24$).

4. Discussion

Poor cage-apophyseal ring contact is an acclaimed risk factor of subsidence in the biomechanical literature (Briski et al., 2017; Deukmedjian et al., 2014; Palepu et al., 2019a; Wang et al., 2023), yet no study thus far has investigated this within a clinical cohort. This study developed a novel biomechanical approach to extract apophyseal ring geometry from routinely captured radiographic images to verify the importance of apophyseal ring contact in vivo. Results showed that poor apophyseal ring contact percentage across the index level is associated with subsidence (≥2 mm), requiring 45.7% (38.4–53.6%) contact at both endplates to achieve a 50% subsidence risk. The RMSE of the calculated apophyseal ring contact percentage is up to 6.3%, which means that prediction uncertainty from inter-sample variance and measurement error are of comparable magnitude. Due to this measurement error, the upper limit of cage-apophyseal ring contact (54%) holds more confidence in exceeding the 50% subsidence risk estimate and thus, may be used as a conservative target in theory, although in practice it should be noted that precision to this level is likely unachievable.

It remains elusive as to what tissue-level property drives the strength increase between the apophyseal ring and core region. Indentation tests have repeatedly demonstrated that the apparent-level stiffness and strength of the peripheral bone is significantly greater than the central region (Grant et al., 2001; Grant et al., 2002; Liu et al., 2016), of which correlates with both the density of the trabecular architecture 6 mm below the endplate (Liu et al., 2016), and endplate cortex thickness (Zhao et al., 2009). In the present study, cortical thickness could not be quantified due to the partial volume effect in radiographic follow-up, but the HU volume 2 mm beneath the cage correlated with apophyseal ring contact percentage. Furthermore, recent evidence has demonstrated that TLIF subsidence force is weakly correlated with the aggressiveness of endplate preparation (Wang et al., 2025) and the endplate thickness after preparation (Palepu et al., 2019a). Taken together, it is likely that resistance to subsidence is also mediated through a stronger scaffold of trabecular bone underlying the apophyseal ring, where failure may originate through strut collapse or permanent deformation of the trabecular structure. Although the cortex strength is a key modulator of stress transfer through the cage-vertebra interface (Polikeit et al., 2003) and should not be disregarded, this interpretation may mitigate the limitation that in this study, any confounding effects of endplate preparation and residual cortex thickness could not be analysed.

The significant effect of index-level apophyseal ring contact percentage across the subsidence categories was lost when considering the suprajacent and subjacent endplate individually (Fig. 3). This suggests that a synergistic effect is revealed when contact is sufficient at both endplates, whereby the subsidence event is influenced by the combined contact status, rather than at an individual endplate. This effect may favour suprajacent endplate contact, where No Subsidence patients exhibited greater cage-apophyseal contact area (Fig. 3B), and both apophyseal ring contact at the suprajacent endplate and the index-level were significant predictors of subsidence occurrence and depth, but not the subjacent (Table 2, Table 3). The superior (subjacent) endplate has been extensively documented for its reduced strength (Liu et al., 2016), bony endplate thickness, and trabecular bone density (Zhao et al., 2009) compared to the inferior (suprajacent), which may enhance susceptibility to cage subsidence irrespective of cage position. Additionally, the

Table 3
– Univariate Pearson correlation coefficients and multivariate standardised Beta coefficients to predict subsidence depth. Note that variables which were not included in the final iteration of multivariate analysis, and covariates which were not considered for univariate analysis, are indicated by a dash. ***P < 0.001, **P < 0.01, *P < 0.05.

	Univariate			Multivariate		
	Suprajacent	Subjacent	Index	Suprajacent	Subjacent	Index
Cage-endplate contact area	−0.332*	−0.298*	−0.523***	–	–	–
Cage-apophyseal ring contact area	−0.444**	−0.409**	−0.491**	–	–	–
Apophyseal ring contact %	−0.371**	−0.304*	−0.357*	–	–	–
Cage length	–	–	–	−0.421**	−0.359*	−0.353*
Centre point ratio	–	–	–	–	−0.339*	−0.327*
L3 HU[1]	–	–	–	−0.324*	–	−0.345**

[1] Hounsfield unit.

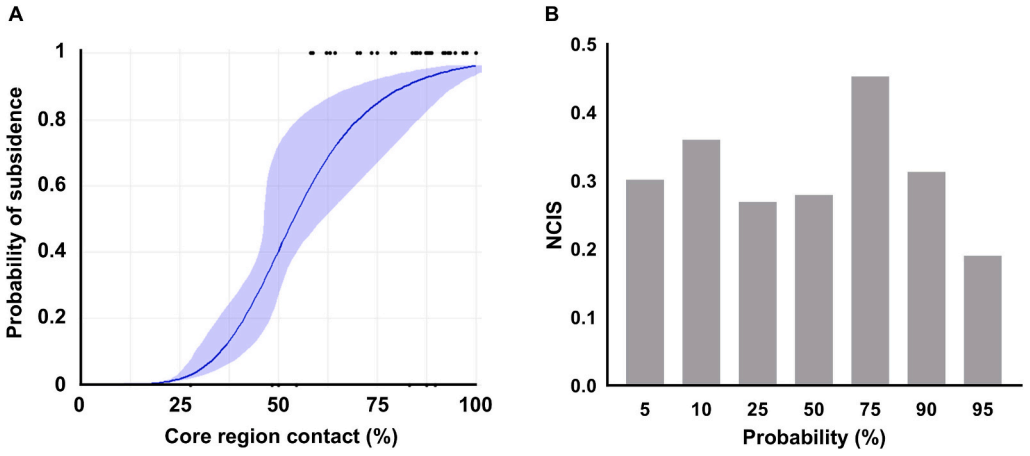


Fig. 4. (A) Injury risk curve of subsidence probability against core region contact percentage (100 – apophyseal ring contact percentage). Shaded region = normalised confidence interval size (NCIS). (B) NCIS for discrete probability intervals.

increased endplate concavity of the suprajacent endplate (van der Houwen et al., 2010) may penalise cage-endplate congruency if the cage is not predominantly resting on the outer rim, which may explain why suprajacent cage-endplate contact was significantly lower for subsidence cases, but there was no effect for subjacent (Fig. 3D,G).

Cage-apophyseal ring contact percentage demonstrated weaker predictive capability of subsidence severity (≥4 mm) compared to incidence (≥2 mm), although it was a significant univariate predictor of subsidence depth (Table 2, Table 3). Conversely, the HU beneath the cage was significantly lower in Severe Subsidence patients relative to No Subsidence, and L3 HU was a significant multivariate predictor of Severe Subsidence (Table 2). There is discordance in prior clinical and biomechanical studies to support this finding. Whilst severe subsidence and subsidence depth has been associated with bone quality (Katz et al., 2024; Levy et al., 2024), the relationship between endplate BMD and cage-endplate interface stiffness has been shown to be non-significant after 5000 loading cycles (Alkalay et al., 2018). This supports other clinical observations of 1-year post-operative subsidence being minimally dependent on bone quality, the latter of which is more crucial in the initiation of intra-operative endplate injury (Satake et al., 2017). Considering this, it is possible that the apophyseal ring resists initial onset of subsidence due to support from the proximal trabecular bone, but after damage has initiated, there is a gradual redundancy of the bone quality in failure propagation. Further work dichotomising intra-operative and post-operative events is needed to establish the role of the underlying trabeculae in subsidence progression.

In addition to L3 HU, cage length and CPR were multivariate predictors of subsidence depth (Table 3). It is well documented that anterior positioning remains optimal for minimising TLIF subsidence risk (Amorim-Barbosa et al., 2022; Fukuta et al., 2011; Levy et al., 2024; Yao et al., 2020). Alongside indirect placement on the apophyseal ring, anterior placement may promote a more stable biomechanical environment (Castellvi et al., 2015; Kwon et al., 2003). Based on this, maximising apophyseal ring contact should not be at the expense of achieving index-level stability through an anteriorly placed cage. It may also be possible that the inflection point at the apophyseal ring-core region boundary creates an unfavourable interface for the cage to settle, where the higher curvature reduces the congruency between the cage and the endplate (Palepu et al., 2019a). Therefore, greater anterior positioning may also represent greater settlement onto the broader, flatter, cortex. Whether this hypothesis applies along the entire boundary of the apophyseal ring is unknown, owing to the nature of this cohort (i.e., absence of deformity correction cases), which meant achievement of anterior-medial cage placement was prioritised intra-operatively. Despite this, sum apophyseal ring contact remained in the multivariate prediction of moderate subsidence, demonstrating its use as an independent risk factor to supplement subsidence prediction.

This study bears a strength in its novel approach to determine the three-dimensional boundary of the apophyseal ring, routinely neglected in radiographic analyses, and may bear particular importance for unilateral approaches. It has been previously attempted to make recommendations on cage type based on apophyseal ring width (Sun et al., 2018). Pre-operative assessment of apophyseal ring surface area may also influence decisions regarding the LIF approach (i.e., patients with limited apophyseal ring surface area may be better suited to approaches whereby the cage footprint is larger).

The inability to quantify cage migration during the post-operative phase could be seen as a significant methodological limitation. During TLIF procedures, as high as 85.1% of patients may exhibit cage migration (Rickert et al., 2023), meaning that the location of the cage quantified in the post-operative CT images may not represent the initial cage placement. Whilst this limitation does not concern the presented results,

as the contact area post-settlement is a true reflection of the interface before a subsidence event, it highlights that pre-and intra-operative efforts to optimise cage placement can be futile due to movement in the post-operative phase. However, Rickert et al. demonstrated that migration events were on average <1 mm and in 90% of cases, <3 mm (Rickert et al., 2023). Therefore, it is unlikely that the apophyseal ring contact would be substantially altered alongside consideration of the error margin observed in this study (± 6.3%).

Additionally, it was not possible to stratify the groups such that an equal number of patients were in each category. The smaller number of No Subsidence patients, whilst inevitable due to the retrospective nature of this study and minimal availability of this patient sub-category, means that caution must be applied when generalising these findings, particularly to cohorts of alternative fusion approaches, where No Subsidence cases are expected to be of greater availability. However, generalisability may be partially restored by the multi-centre study design, which controls bias introduced by surgeon technique. Furthermore, a post-hoc power analysis (G*Power v3.1.9.7 (Faul et al., 2007)) accounting for these unequal groupings demonstrated that the power to detect statistical changes in apophyseal ring contact percentage was 0.83 (Cohen's f: 0.53, $\alpha = 0.05$), which is considered sufficient upon consideration with additional multivariate analyses.

Another limitation was the definition of cage-endplate contact area, which did not account for micro-scale incongruencies of endplate and the cage due to irregular endplate topology. Contact area instead relied on the macroscopic endplate profile at the retrospectively-inferred cage position. Due to this, it is possible that contact area was over-estimated in subsidence cases, as cage settling reduced the cage-endplate mismatch. However, contact area was still significantly lower in Severe Subsidence relative to No Subsidence, demonstrating that the effect size was larger than potential bias arising in subsidence cases.

5. Conclusions

This study highlights that contact between the cage and the apophyseal ring may be an important consideration when predicting risk of subsidence following TLIF. However, the association with severe subsidence remains unclear. Based on this study, it is recommended that at least 54% of the cage should contact the apophyseal ring as a conservative target, with particular attention given to the suprajacent endplate.

CRediT authorship contribution statement

Kay A. Raftery: Writing – review & editing, Writing – original draft, Visualization, Validation, Methodology, Investigation, Formal analysis, Data curation, Conceptualization. **Hannah Levy:** Writing – review & editing, Resources, Project administration, Methodology, Investigation, Conceptualization. **Lea Adamson:** Writing – review & editing, Validation, Investigation, Data curation. **Christopher Magera:** Writing – review & editing, Resources, Project administration, Data curation. **Brett Freedman:** Writing – review & editing, Supervision, Resources, Project administration, Investigation, Conceptualization. **Nicolas Newell:** Writing – review & editing, Supervision, Resources, Project administration, Conceptualization.

Funding statement

This research did not receive any specific grant from funding agencies in the public, commercial, or not-for-profit sectors.

Declaration of competing interest

The authors declare the following financial interests/personal relationships which may be considered as potential competing interests: Brett Freedman reports a relationship with Clear Choice Therapeutics that includes: equity or stocks. Brett Freedman reports a relationship with Medtronic Inc. that includes: consulting or advisory. Brett Freedman reports a relationship with DePuy Synthes that includes: consulting or advisory and speaking and lecture fees. Brett Freedman reports a relationship with Kuros Biosciences Usa, Inc. that includes: consulting or advisory. Brett Freedman reports a relationship with Amgen that includes: consulting or advisory and speaking and lecture fees. Brett Freedman reports a relationship with Theradaptive that includes: board membership. If there are other authors, they declare that they have no known competing financial interests or personal relationships that could have appeared to influence the work reported in this paper.

Appendix A. Supplementary data

Supplementary data to this article can be found online at https://doi.org/10.1016/j.clinbiomech.2026.106792.

References

Alkalay, R.N., Adamson, R., Groff, M.W., 2018. The effect of interbody fusion cage design on the stability of the instrumented spine in response to cyclic loading: an experimental study. Spine J. 18 (10). https://doi.org/10.1016/j.spinee.2018.03.003.

Amorim-Barbosa, T., Pereira, C., Catelas, D., et al., 2022. Risk factors for cage subsidence and clinical outcomes after transforaminal and posterior lumbar interbody fusion. Eur. J. Orthop. Surg. Traumatol. 32 (7). https://doi.org/10.1007/s00590-021-03103-z.

Andriamifidy, H.F., Rohde, M., Swami, P., Liang, H., Grande, D., Virk, S., 2024. Influence of placement of lumbar interbody cage on subsidence risk: biomechanical study. World Neurosurg. 183. https://doi.org/10.1016/j.wneu.2023.12.118.

Briski, D.C., Goel, V.K., Waddell, B.S., et al., 2017. Does spanning a lateral lumbar interbody cage across the vertebral ring apophysis increase loads required for failure and mitigate endplate violation. Spine (Phila Pa 1976) 42 (20). https://doi.org/10.1097/BRS.0000000000002158.

Castellvi, A.D., Thampi, S.K., Cook, D.J., et al., 2015. Effect of TLIF cage placement on in vivo kinematics. Int. J. Spine Surg. 9. https://doi.org/10.14444/2038.

Chen, L., Yang, H., Tang, T., 2005. Cage migration in spondylolisthesis treated with posterior lumbar interbody fusion using BAK cages. Spine (Phila Pa 1976) 30 (19). https://doi.org/10.1097/01.brs.0000180402.50500.5b.

Choi, J.Y., Sung, K.H., 2006. Subsidence after anterior lumbar interbody fusion using paired stand-alone rectangular cages. Eur. Spine J. 15 (1). https://doi.org/10.1007/s00586-004-0817-y.

Deukmedjian, A.R., Manwaring, J., Le, T.V., Turner, A.W.L., Uribe, J.S., 2014. Corpectomy cage subsidence with rectangular versus round endcaps. J. Clin. Neurosci. 21 (9). https://doi.org/10.1016/j.jocn.2013.12.028.

Di, M., Weng, Y., Wang, G., et al., 2023. Cortical endplate bone density measured by novel Phantomless quantitative computed tomography may predict cage subsidence more conveniently and accurately. Orthop. Surg. 15 (12), 3126–3135. https://doi.org/10.1111/os.13897.

Faul, F., Erdfelder, E., Lang, A.G., Buchner, A., 2007. G*power 3: a flexible statistical power analysis program for the social, behavioral, and biomedical sciences. Behav. Res. Methods 39. https://doi.org/10.3758/BF03193146.

Fukuta, S., Miyamoto, K., Hosoe, H., Shimizu, K., 2011. Kidney-type intervertebral spacers should be located anteriorly in cantilever transforaminal lumbar interbody fusion: analyses of risk factors for spacer subsidence for a minimum of 2 years. J. Spinal Disord. Tech. 24 (3). https://doi.org/10.1097/BSD.0b013e3181e9f249.

Fyhrie, D.P., Schaffler, M.B., 1994. Failure mechanisms in human vertebral cancellous bone. Bone 15 (1). https://doi.org/10.1016/8756-3282(94)90900-8.

Grant, J.P., Oxland, T.R., Dvorak, M.F., 2001. Mapping the structural properties of the lumbosacral vertebral endplates. Spine 26. https://doi.org/10.1097/00007632-200104150-00012.

Grant, J.P., Oxland, T.R., Dvorak, M.F., Fisher, C.G., 2002. The effects of bone density and disc degeneration on the structural property distributions in the lower lumbar vertebral endplates. J. Orthop. Res. 20 (5). https://doi.org/10.1016/S0736-0266(02)00039-6.

Hu, Y.H., Niu, C.C., Hsieh, M.K., Tsai, T.T., Chen, W.J., Lai, P.L., 2019. Cage positioning as a risk factor for posterior cage migration following transforaminal lumbar interbody fusion - an analysis of 953 cases. BMC Musculoskelet. Disord. 20 (1). https://doi.org/10.1186/s12891-019-2630-0.

Katz, A.D., Song, J., Duvvuri, P., et al., 2024. Bone density correlates with depth of subsidence after expandable interbody cage placement. Clin. Spine Surg. https://doi.org/10.1097/BSD.0000000000001727. Published online November 21.

Koo, T.K., Li, M.Y., 2016. A guideline of selecting and reporting Intraclass correlation coefficients for reliability research. J. Chiropr. Med. 15 (2). https://doi.org/10.1016/j.jcm.2016.02.012.

Kwon, B.K., Berta, S., Daffner, S.D., et al., 2003. Radiographic analysis of Transforaminal lumbar interbody fusion for the treatment of adult isthmic spondylolisthesis. J. Spinal Disord. Tech. 16 (5). https://doi.org/10.1097/00024720-200310000-00006.

Lee, N., Kim, K.N., Yi, S., et al., 2017. Comparison of outcomes of anterior, posterior, and transforaminal lumbar interbody fusion surgery at a single lumbar level with degenerative spinal disease. World Neurosurg. 101. https://doi.org/10.1016/j.wneu.2017.01.114.

Levy, H.A., Hamouda, A.M., Magera, C.A., et al., 2025. Do Three-Dimensional Printed Porous Titanium Relative to Polyetheretherketone Interbody Cages Reduce Complications and Revisions after Transforaminal Lumbar Interbody Fusion? Global Spine J 16 (1). https://doi.org/10.1177/21925682251339998.

Levy, H.A., Pinter, Z.W., Reed, R., et al., 2024. Transforaminal lumbar interbody fusion subsidence: computed tomography analysis of incidence, associated risk factors, and impact on outcomes. J. Neurosurg. Spine 1–10. https://doi.org/10.3171/2024.4.SPINE231007. Published online July 1.

Lin, G.X., Akbary, K., Kotheeranurak, V., et al., 2018. Clinical and radiologic outcomes of direct versus indirect decompression with lumbar interbody fusion: a matched-pair comparison analysis. World Neurosurg. 119. https://doi.org/10.1016/j.wneu.2018.08.003.

Liu, J., Hao, L., Suyou, L., et al., 2016. Biomechanical properties of lumbar endplates and their correlation with MRI findings of lumbar degeneration. J. Biomech. 49 (4). https://doi.org/10.1016/j.jbiomech.2016.01.019.

Maniadakis, N., Gray, A., 2000. The economic burden of back pain in the UK. Pain 84 (1). https://doi.org/10.1016/S0304-3959(99)00187-6.

Mobbs, R., Phan, K., Malham, G., et al., 2015. Lumbar interbody fusion: techniques, indications and comparison of interbody fusion options including PLIF, TLIF, MI-TLIF, OLIF/ATP, LLIF and ALIF. J. Spine Surg. https://doi.org/10.3978/j.issn.2414-469X.2015.10.05. Published online.

Muntoni, A., Cignoni, P., 2025. PyMeshLab. Zenodo. https://doi.org/10.5281/zenodo.4438750. Preprint posted online 2021.

Palepu, V., Helgeson, M.D., Molyneaux-Francis, M., Nagaraja, S., 2019a. The effects of bone microstructure on subsidence risk for ALIF, LLIF, PLIF, and TLIF spine cages. J. Biomech. Eng. 141 (3). https://doi.org/10.1115/1.4042181.

Palepu, V., Rayaprolu, S.D., Nagaraja, S., 2019b. Differences in trabecular bone, cortical shell, and endplate microstructure across the lumbar spine. Int. J. Spine Surg. 13 (4). https://doi.org/10.14444/6049.

Petitjean, A., Trosseille, X., Yoganandan, N., Pintar, F.A., 2015. Normalization and Scaling for Human Response Corridors and Development of Injury Risk Curves. https://doi.org/10.1007/978-1-4939-1732-7_26.

Pinter, Z.W., Reed, R., Townsley, S.E., et al., 2023a. Titanium cervical cage subsidence: postoperative computed tomography analysis defining incidence and associated risk factors. Glob. Spine J. 13 (7). https://doi.org/10.1177/21925682211046897.

Pinter, Z.W., Mikula, A., Shirley, M., et al., 2023b. Risk factors for allograft subsidence following anterior cervical discectomy and fusion. World Neurosurg. 170. https://doi.org/10.1016/j.wneu.2022.11.109.

Polikeit, A., Ferguson, S.J., Nolte, L.P., Orr, T.E., 2003. The importance of the endplate for interbody cages in the lumbar spine. Eur. Spine J. 12 (6), 556–561. https://doi.org/10.1007/s00586-003-0556-5.

Provaggi, E., Capelli, C., Leong, J.J.H., Kalaskar, D.M., 2018. A UK-based pilot study of current surgical practice and implant preferences in lumbar fusion surgery. Medicine 97 (26), e11169. https://doi.org/10.1097/MD.0000000000011169.

Rickert, M., Fennema, P., Wehner, D., et al., 2023. Postoperative cage migration and subsidence following TLIF surgery is not associated with bony fusion. Sci. Rep. 13 (1). https://doi.org/10.1038/s41598-023-38801-7.

Rushton, A., White, L., Heap, A., Heneghan, N., 2015. Evaluation of current surgeon practice for patients undergoing lumbar spinal fusion surgery in the United Kingdom. World J. Orthop. 6 (6). https://doi.org/10.5312/wjo.v6.i6.483.

Satake, K., Kanemura, T., Nakashima, H., Yamaguchi, H., Segi, N., Ouchida, J., 2017. Cage subsidence in lateral interbody fusion with transpsoas approach: intraoperative endplate injury or late-onset settling. Spine Surg. Relat. Res. 1 (4). https://doi.org/10.22603/ssrr.1.2017-0004.

Sivasubramaniam, V., Patel, H.C., Ozdemir, B.A., Papadopoulos, M.C., 2015. Trends in hospital admissions and surgical procedures for degenerative lumbar spine disease in England: a 15-year time-series study. BMJ Open 5 (12), e009011. https://doi.org/10.1136/bmjopen-2015-009011.

Sun, C., Wang, H., Jiang, J., Lu, F., Ma, X., Xia, X., 2018. Length of lumbar interbody cage using radiological measurements of Chinese endplates and the apophyseal ring. World Neurosurg. 116. https://doi.org/10.1016/j.wneu.2018.05.234.

van der Houwen, E.B., Baron, P., Veldhuizen, A.G., Burgerhof, J.G.M., van Ooijen, P.M.A., Verkerke, G.J., 2010. Geometry of the intervertebral volume and vertebral endplates of the human spine. Ann. Biomed. Eng. 38 (1), 33–40. https://doi.org/10.1007/s10439-009-9827-6.

von Elm, E., Altman, D.G., Egger, M., Pocock, S.J., Gøtzsche, P.C., Vandenbroucke, J.P., 2014. The strengthening the reporting of observational studies in epidemiology (STROBE) statement: guidelines for reporting observational studies. Int. J. Surg. 12 (12). https://doi.org/10.1016/j.ijsu.2014.07.013.

Wang, J., Geng, Z., Wu, J., et al., 2023. Biomechanical properties of lumbar vertebral ring apophysis cage under endplate injury: a finite element analysis. BMC Musculoskelet. Disord. 24 (1). https://doi.org/10.1186/s12891-023-06792-1.

Wang, W.P., Slater, T.D., Raftery, K.A., et al., 2025. Endplate preparation for anterior cervical discectomy and fusion: does the amount of endplate removed affect cage subsidence risk? Eur. Spine J. 34, 3294–3303. https://doi.org/10.1007/s00586-025-08997-5.

Yao, Y.C., Chou, P.H., Lin, H.H., Wang, S.T., Liu, C.L., Chang, M.C., 2020. Risk factors of cage subsidence in patients received minimally invasive transforaminal lumbar interbody fusion. Spine (Phila Pa 1976) 45 (19). https://doi.org/10.1097/BRS.0000000000003557.

Yoganandan, N., Moore, J., DeVogel, N., et al., 2020. Human lumbar spinal column injury criteria from vertical loading at the base: applications to military environments. J. Mech. Behav. Biomed. Mater. 105. https://doi.org/10.1016/j.jmbbm.2020.103690.

Yoo, S.J., Kim, K.H., Chin, D.K., Kim, K.S., Cho, Y.E., Park, J.Y., 2022. Minimally invasive versus conventional lumbar interbody fusion at L5–S1: a retrospective comparative study. J. Minim. Invasive Spine Surg. Tech. 7 (1), 37–45. https://doi.org/10.21182/jmisst.2022.00472.

Zhang, Y., Nüesch, C., Mündermann, A., Halbeisen, F., Schären, S., Netzer, C., 2025. Is age a risk factor for early postoperative cage subsidence after Transforaminal lumbar interbody fusion? A retrospective study in 170 patients. Global Spine J. 15 (2), 940–948. https://doi.org/10.1177/21925682231217692.

Zhao, F.D., Pollintine, P., Hole, B.D., Adams, M.A., Dolan, P., 2009. Vertebral fractures usually affect the cranial endplate because it is thinner and supported by less-dense trabecular bone. Bone 44 (2). https://doi.org/10.1016/j.bone.2008.10.048.

Glossary

Endplate: the bony interface between the vertebral body and the intervertebral disc
Apophyseal ring: peripheral rim of cortical bone on the vertebral endplate
Subsidence: excessive settling of the interbody cage into the vertebral body
Interbody cage: an implant used in spinal fusion procedures to house bone graft and encourage bony fusion between the two adjacent vertebra
Footprint: surface area of implant which engages with the vertebral bone
Suprajacent endplate: the endplate immediately above, or cranial to, the implant in space
Subjacent endplate: the endplate immediately below, or caudal to, the implant in space